Magnetic Resonance in Medicine 69:1408–1420 (2013)

Phase-Sensitive Inversion Recovery for Myocardial T_1 Mapping with Motion Correction and Parametric Fitting

Hui Xue,[1]* Andreas Greiser,[2] Sven Zuehlsdorff,[3] Marie-Pierre Jolly,[1] Jens Guehring,[2] Andrew E. Arai,[4] and Peter Kellman[4]

The assessment of myocardial fibrosis and extracellular volume requires accurate estimation of myocardial T_1s. While image acquisition using the modified Look-Locker inversion recovery technique is clinically feasible for myocardial T_1 mapping, respiratory motion can limit its applicability. Moreover, the conventional T_1 fitting approach using the magnitude inversion recovery images can lead to less stable T_1 estimates and increased computational cost. In this article, we propose a novel T_1 mapping scheme that is based on phase-sensitive image reconstruction and the restoration of polarity of the MR signal after inversion. The motion correction is achieved by registering the reconstructed images after background phase removal. The restored signal polarity of the inversion recovery signal helps the T_1 fitting resulting in improved quality of the T_1 map and reducing the computational cost. Quantitative validation on a data cohort of 45 patients proves the robustness of the proposed method against varying image contrast. Compared to the magnitude T_1 fitting, the proposed phase-sensitive method leads to less fluctuation in T_1 estimates. **Magn Reson Med 69:1408–1420, 2013. © 2012 Wiley Periodicals, Inc.**

Key words: T_1 mapping; phase-sensitive inversion recovery; motion correction; MOLLI; cardiac MRI

INTRODUCTION

Recent progress in MR cardiac imaging enables myocardial T_1 mapping with multiple heartbeats. The basic imaging sequences rely on inverting the magnetization and acquiring images along the longitudinal recovery curve. Examples include the modified Look-Locker inversion recovery (MOLLI) (1,2) and variations such as shortened-MOLLI (3,4). Unlike T_1 mapping in neuroskeletal or musculoskeletal imaging applications (5,6), the inversion recovery curves of the myocardium typically cannot be uniformly sampled with a fixed interval, because the native T_1 value of myocardium is around 950 ms at 1.5 T, which is on the order of typical cardiac cycle (7). In order to sample the inversion recovery curve and subsequently estimate T_1 values with sufficient precision, as shown in Fig. 1, 5 to 11 images are typically acquired at different inversion times (TIs), which are electrocardiography (ECG) triggered with imaging at a mid-diastolic phase. The maximal number of MOLLI samples is constrained by the breath-hold duration that is viable in a clinical workflow (1,4,8).

Respiratory motion often occurs despite breath-holding due to either diaphragmatic drift or the patient's inability or noncompliance to hold the breath. In a previous study (9) involving 50 consecutive patients who underwent MOLLI imaging, 230 MOLLI series were acquired for both precontrast and postcontrast scenarios. Noticeable motion was found in 40% of all acquired datasets. This undesired respiratory motion can lead to errors in the pixel-wise estimation of T_1 maps, and motion correction is necessary to maximize the clinical robustness of myocardial T_1-mapping.

The main challenge of robust myocardial motion correction using image registration in inversion recovery images is the dramatic variation in image contrast (9), because the MR signal of different tissue (e.g., blood, fat, myocardium, infarcted tissue) will be nulled at different TIs due to different specific T_1s. In particular, the contrast between different tissues can change or even invert with the TIs.

Previously published myocardial T_1 mapping techniques utilize magnitude-reconstructed images (1,4,9), which means the signal intensity used for inversion recovery fitting is the magnitude of complex signal and does not contain information on polarity of the magnetization. As shown in Fig. 2, given the magnitude detection of MOLLI images, for the precontrast cases, the signal of blood is higher than the myocardium shortly after inversion. At longer TIs, the contrast is inverted, and the signal of myocardium is higher. In the postcontrast imaging, due to the injection of T_1 shortening contrast agent, the blood signal can be lower than the myocardium for short TIs; for longer TIs, the blood become brighter. This contrast inversion causes a dramatic change in image appearance that appears to be the major challenge for registration algorithms; even state of the art registration approaches using information-based metrics can result in suboptimal alignment (9). On the other hand, as illustrated in Fig. 2, if the real part of the phase-sensitive reconstructed image (not its magnitude) is considered, the contrast inversion can be completely avoided. The image registration can be further compounded by partial volume cancellation at the boundaries between tissues of different T_1s. Because of the number of tissue types in the field of view, it is not practical to find a set of TI that can avoid these problems.

[1]Siemens Corporation, Corporate Research, Princeton, New Jersey, USA.
[2]Imaging and Therapy Division, Siemens AG, Healthcare Sector, Erlangen, Germany.
[3]CMR R&D, Siemens Healthcare USA, Inc., Chicago, Illinois, USA.
[4]Laboratory of Cardiac Energetics, National Heart, Lung and Blood Institute, National Institutes of Health, Bethesda, Maryland, USA.
*Correspondence to: Hui Xue, Ph.D., Siemens Corporation, Corporate Research, 755 College Road East, Princeton, NJ 08540 USA. E-mail: huiue@siemens.com
Received 6 March 2012; revised 27 May 2012; accepted 29 May 2012.
DOI 10.1002/mrm.24385
Published online 26 June 2012 in Wiley Online Library (wileyonlinelibrary.com).

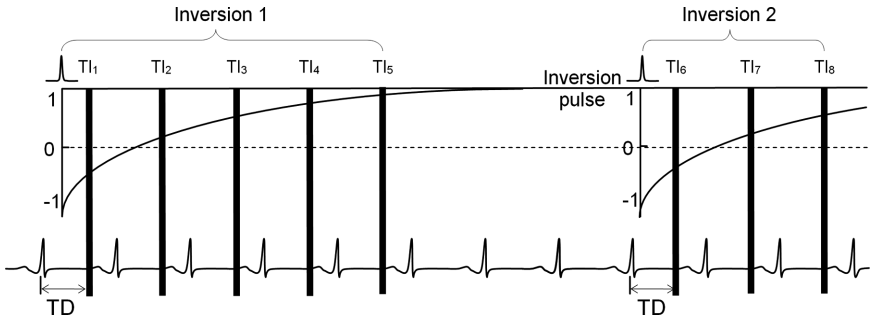

FIG. 1. A MOLLI sequence scheme showing two sets of Look-Locker experiments were performed with increasing TI within one breath-hold. A total of eight images are acquired, as shown by the vertical bar. Images were acquired with the specific trigger delay (TD) selected for imaging at mid-diastole. Each *R–R* interval is measured, and the actual values of TI are used for T_1-mapping. In this scheme, five images are acquired during the first inversion recovery and three are acquired from the second inversion recovery.

The use of magnitude-reconstructed images for T_1 fitting poses additional challenges. In order to fit an inversion recovery signal model (e.g., the three-parameter model; Ref. 10) to the signal curve, it is necessary to identify the data points that shall be inverted to recover signal polarity. As proposed in Ref. 11, the signal polarity can be estimated by the multifitting inversion recovery method (MF-MAGIR). This approach performs an initial fit assuming that all data points are positive; a subsequent fit inverts the first data point, the third fit inverts the first two points, and so on. Finally, the fit with the lowest residual error is selected. Although this strategy is more robust than a direct fit to the magnitude without polarity recovery, the need for multiple trials leads to linearly increasing computational costs. If the pixel-wise T_1 map is estimated, the multifitting needs to be performed for every pixel in the field of view, and significant computational time will be spent on performing trial fits. Second, the signal-to-noise ratio of inversion recovery images near the signal null is low and therefore the signal can be biased by the noise magnitude, which can lead to errors in T_1s. Furthermore, data points around signal nulling may lead to ambiguity in polarity recovery, thus increases the variance of the estimated T_1. Finally, the selection of TI times can influence the signal recovery curve. For pixels with extreme T_1s, the magnetization may not even cross zero for the specific TIs. This can cause the failure of multifitting approach.

Recently, a synthetic image estimation based motion correction (SynMOCO) approach was proposed to effectively register individual MOLLI images (9). This method addresses the problem of large variation of image contrast by estimating motion-free synthetic images by solving an energy minimization problem. These synthetic images present similar contrast to the acquired MOLLI images at every TI. The myocardial motion is finally corrected by registering every MOLLI image to its corresponding synthetic image. This method still utilizes the time-consuming MF-MAGIR method to estimate T_1s, and its complexity is further increased by the synthetic image estimation step.

To address the challenges caused by the magnitude detection, in this study we propose a novel motion correction and T_1 mapping scheme using phase-sensitive inversion recovery (PSIR) reconstruction. The proposed

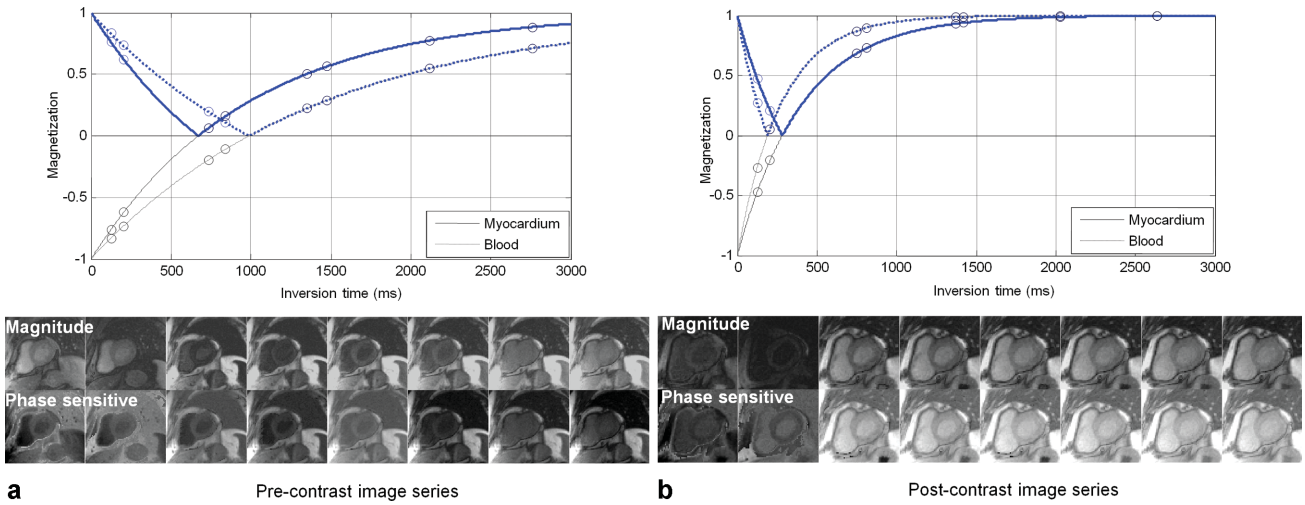

FIG. 2. Precontrast and postcontrast image series acquired using the MOLLI sequences. The magnitude images and corresponding phase-sensitive images are plotted together with the inversion recovery signal curves for blood and myocardium. The magnitude images of precontrast series show that the blood is first brighter then darker than myocardium, while in the phase-sensitive images, the blood is darker than myocardium. Thus, the phase-sensitive detection eliminates the blood–myocardium contrast inversion. The similar phenomenon can be observed in postcontrast images, where the blood is brighter than myocardium due to the injection of contrast agent.

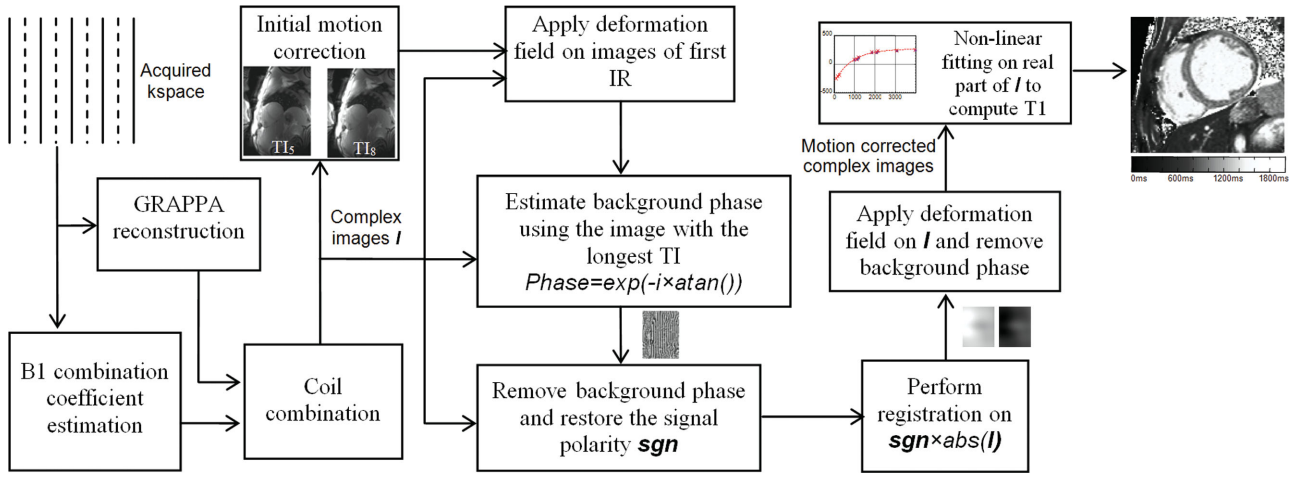

FIG. 3. Flow chart of phase-sensitive inversion recovery MOLLI mapping with motion correction and nonlinear parametric fitting. [Color figure can be viewed in the online issue, which is available at wileyonlinelibrary.com.]

approach produces inversion recovery signal with known polarity to remove the background phase while preserving the polarity of inversion recovery magnetization. Because the background phases are often contaminated by noises and field inhomogeneity, the real part of reconstructed complex images may not reflect the correct magnitude and polarity of inversion magnetization. Similar to the well established phase-sensitive delayed enhancement imaging (12), PSIR reconstruction is needed to preserve the polarity of magnetization by removing contaminating background phase errors. Because the PSIR-reconstructed images do not exhibit the contrast inversion appearing in magnitude images, the need for multiple fitting is eliminated and the possible confusion of whether to invert data points near signal nulling is avoided. This can lead to an improved T_1 map with less fitting errors. The effectiveness of the proposed technique was verified in vivo on a large cohort of patient datasets. We will show that the PSIR motion correction (PSIR-MOCO) is capable of correcting MOLLI images with different motion patterns and contrast concentrations. While the SynMOCO method achieves similar motion correction accuracy, the PSIR-MOCO is conceptually simpler and computationally faster. With the correction of myocardial motion and restoration of signal polarity, the PSIR fitting improves the quality of T_1 map.

METHODS

We propose to perform myocardial T_1 mapping by exploiting the phase-sensitive image reconstruction. This approach exploits the fact that the MOLLI image with long TI has well recovered magnetization; therefore, the phase of this image can be used to restore the signal polarity for the entire MOLLI series. In this way, the varying image contrast during the MOLLI series can be removed, and registering MOLLI frames becomes robust. Moreover, the fitting on MOLLI signals with restored polarity is more efficient and leads to better T_1 maps with less erroneous fluctuation. Figure 3 illustrates the entire process, including phase-sensitive reconstruction, motion correction, and inversion recovery fitting.

Phase-Sensitive Image Reconstruction

The benefits of phase-sensitive reconstruction for cardiac imaging have been well accepted for the delayed enhancement imaging of infarction (12). In PSIR-delayed enhancement imaging (12), an extra proton density (PD) image is acquired besides the inversion recovery (IR) image. This proton density image is used as the source for background phase estimation. In the proposed PSIR MOLLI reconstruction, the phase reference image is selected as the image with the longest TI, which has sufficiently recovered magnetization.

As the first step, complex images are reconstructed using parallel imaging with generalized autocalibrating partially parallel acquisitions (GRAPPA) acceleration factor 2, and individual coil images are adaptively combined to produce a single complex image for each TI. The MOLLI image with the longest TI is used to remove the background phase of all MOLLI images on a pixel-by-pixel basis. The real part of resulting image has the correct polarity of IR signal. Although the phase is spatially smooth in general, the initial misalignment between MOLLI images may still lower the accuracy of background phase removal. To alleviate its influence on registration, an initial motion correction is applied between the last images of every IR experiments. In the current protocol with two inversions, the last image of the first IR is coregistered to the last image of the second IR. These two images have similar contrast because of sufficiently long TIs but can have noticeable misalignment as they are acquired six heartbeats apart. The deformation fields are applied to all other images of the first IR, leading to a reduction in phase error (Fig. 4).

Motion Correction of MOLLI Series

Given the MOLLI images with signal polarity restored, robust motion correction can be achieved by registering the MOLLI images in a frame-by-frame manner, since the contrast inversion is removed. Because of the nonrigid nature of cardiac deformation, a fast variational nonrigid image registration framework (13,14) is applied. In this framework, a dense deformation field is estimated as the

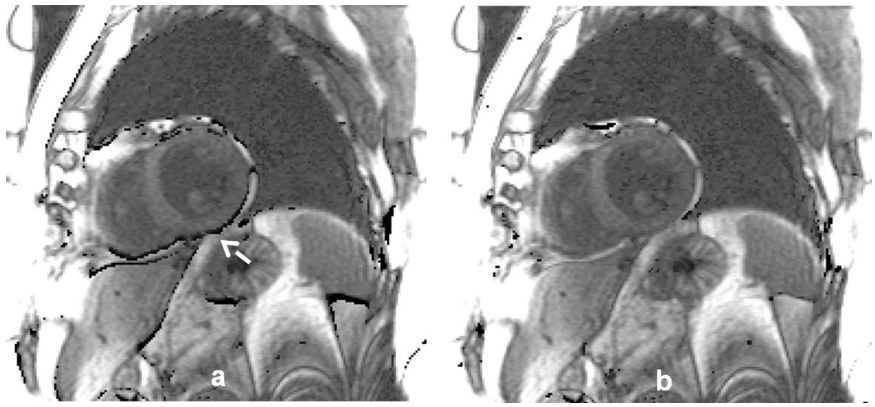

FIG. 4. Initial registration leads to reduced errors in the phase-sensitive images. **a**: A MOLLI phase-sensitive frame without the initial registration. **b**: The same frame after applying the deformation fields of initial registration. The abrupt intensity changes in the phase-sensitive images are reduced.

solution to a calculus of variation problem. It is solved by performing compositional update steps for a partial differential transport equation. The regularization is added by low-pass filtering the gradient images of the cost function. The outcomes are used as velocity field to drive the transport equation. To speed up the convergence and avoid local minima, a multiscale image pyramid is created. The local cross-correlation is used as the image similarity measure, as its explicit derivative can be more efficiently calculated than mutual information and still be general enough to cope with noise and intensity difference between PSIR MOLLI images.

PSIR T_1 Fitting

After motion correction, the deformation field is used to warp the original complex MOLLI images, and the phase of IR image with the longest TI is removed from all images. The motion-corrected complex inversion recovery signal is first phase corrected and the real part of the resulting complex signal is extracted for T_1 fitting. The T_1 map is generated via the pixel-wise curve fitting using the three-parameter signal model (10):

$$\begin{aligned} S(x,y,t_n) &= A(x,y) - B(x,y) \times \exp(-t_n/T_1^*(x,y)) \\ T_1(x,y) &= T_1^*(x,y) \times (B(x,y)/A(x,y) - 1) \end{aligned} \quad [1]$$

where A, B, and T_1^* are estimated by a three-parameter nonlinear fit to the measured data with restored polarity. Here t is the accumulative time from the inversion pulse. T_1^* is the apparent, modified T_1 in an IR experiment. Figure 5 demonstrates the advantages of PSIR T_1 fitting for both precontrast and postcontrast cases. For the precontrast case of this example (Fig. 5a), the MF-MAGIR fitting needs four trials to find the best TI, while the phase-sensitive reconstruction already provides this information. Also, the confusion of whether to invert the points near the signal nulling leads to errors in MF-MAGIR fitting. For this postcontrast case (Fig. 5b), the T_1 is so short in the blood pool that the MF-MAGIR fitting is confused by whether to invert the first sample, while the PSIR fitting ensures the correct polarity of the first data point (in this example, assigning all data points as "positive" leads to lower fitting residual (155.0), while inverting the first data point gives higher residual (176.7); thus the MF-MAGIR fitting which always favor the minimal residual cannot make the correct polarity assignment and gives underestimated T_1). As a result, the increased ambiguity in MF-MAGIR fitting leads to a noisy T_1 map, especially for postcontrast cases where the magnetization generally crosses zero earlier due to shortened T_1s.

Other means to avoid multiple trial fitting could include directly performing the fitting on the magnitude of inversion recovery signal $\left|A(x,y) - B(x,y) \times \exp(-t_n/T_1^*(x,y))\right|$ without trying to detect the polarity. This strategy is hereby named as MAGIR fitting to be differentiated from the multifit magnitude (MF-MAGIR) method. The major drawback of this strategy is that for the postcontrast imaging with shortened T_1 values, there may be insufficient number of data samples before the signal nulling. This often leads to the failed fitting (Fig. 6c,d). Because the T_1 shortening is compounded by the dose of injected contrast, heart rate, blood flow, and other physiological and physical parameters, it is difficult to optimize the protocol to completely avoid this phenomenon. In our experiments, the MAGIR fitting frequently failed for postcontrast cases and gave inferior results on precontrast cases.

Figure 7 illustrates the benefits of motion correction and PSIR fitting. In this precontrast case, the motion correction is able to improve the boundary sharpness of the T_1 map. Compared to the MF-MAGIR fitting, the PSIR fitting further improves the homogeneity of T_1 estimation. The plots of fitting residuals (Fig. 7d–f) show the reduced least square error after motion correction and the PSIR fitting, which corresponds to the improved T_1 estimation shown in the map (Fig. 7c).

The downhill simplex minimization algorithm proposed by Nelder and Mead (so-called Nelder–Mead method; Ref. 15) is applied in all experiments and gives similar outputs as the Levenberg-Marquardt minimization (16), while the Nelder–Mead method is more efficient since only function evaluations are required. The maximal intensity was used to initialize A, approximating the fully recovered magnetization. B was initialized as A minus the minimal intensity, approximating the magnetization at $t_n = 0$. T_1^* was initialized as the linearly interpolated zero-crossing time estimated from the polarity corrected signal intensity curve.

Imaging Experiments

Imaging experiments were performed on 1.5T clinical MRI systems (MAGNETOM Espree and MAGNETOM Avanto, Siemens AG Healthcare Sector, Erlangen,

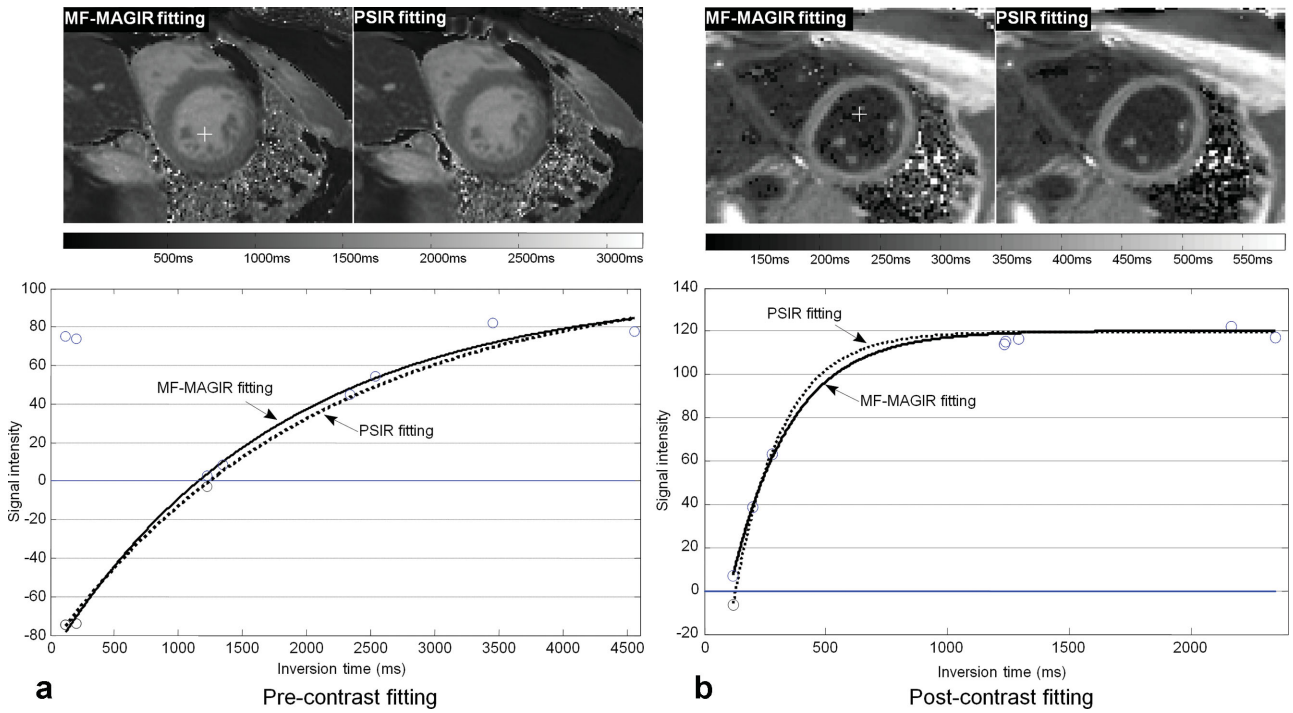

FIG. 5. MOLLI inversion recovery signal curves with MF-MAGIR and PSIR fitting. The phase-sensitive fitting does not require the multiple trials to find the polarity for every data point. For data samples near the signal nulling, the incorrect determination of signal polarity can lead to reduced accuracy in T_1 estimation. **a**: T_1 map of a precontrast MOLLI dataset. For the pixel marked by the white cross, estimated signal curves are plotted for MF-MAGIR and PSIR fitting. Note the phase-sensitive fitting resolves the signal polarity for the third and fourth data points. **b**: T_1 map of a postcontrast MOLLI dataset with shortened T_1s. For the marked pixel, the MF-MAGIR fitting did not find a zero-crossing and incorrectly gave "positive" signs to all data points, including the first one (Note in this example, giving all data points "positive sign" leads to a lower residual of 155.0, while inverting the first data point has a higher residual of 176.7). This gives the fitting results shown by the solid line. With the PSIR fitting, the sign of first data point is correctly assigned as "negative." This leads to the fitting curve shown by the dash line. The T_1 maps show the PSIR fitting is correct and leads to improved estimates. In this case, the MF-MAGIR fitting does give a reasonable recovery curve; however, the resulting T_1 value is inaccurate due to the misassigned signal polarity for the first data point.

Germany) equipped with 32 receiver channels. All subjects were scanned at the National Heart, Lung and Blood Institute, Bethesda, MD. This study was approved by the local Institutional Review Board, and written informed consent was given by all participants.

A total of 45 patients (23 men, 22 women; mean age 47.1 ± 15.9 years) were imaged both before and after contrast injection. Typical sequence parameters are as follows: inversion recovery-prepared MOLLI with balanced steady-state free precession (SSFP) readout, repetition time = 2.4/echo time = 1.05 ms, acquired matrix 192 × 126, reconstructed matrix size 192 × 144, flip angle 35°, in-plane spatial resolution 1.9 × 2.1 mm^2, rectangular FOV 360 × 270 mm^2, slice thickness 6 mm, bandwidth 1000 Hz/pixel. A total of 8 images were acquired with 11 heartbeats using two inversions. All acquisitions were ECG-gated and breath-held.

For every patient, the MOLLI imaging was performed for at least two slices (mid-ventricular short axis and four chamber long axis views) for both precontrast and postcontrast. The postcontrast acquisition was performed at approximately 15–20 min following the intravenous injection of Gd-diethylene triamine pentaacetic acid (DTPA) at 0.15 mmol/kg dose. The entire data cohort consists of 180 MOLLI series (90/90 precontrast/postcontrast, 95/85 short/long axis).

The proposed workflow was implemented using C++. All computations were performed on a 64-bit Window 7 workstation containing two quad-core Intel Xeon E5620 2.4 GHz processors and 24GB RAM. Typical processing time of PSIR-MOCO and fitting was less than 5 s per slice, including initial motion correction, background phase removal, MOLLI image registration, and pixel-wise PSIR T_1 fitting. The computational time is measured by recording the processing time per MOLLI series and computing the mean and standard deviation (STD) for all series.

Quantification of Motion Correction

All MOLLI series were first converted to animated movie files and viewed by an experienced reader who classified all datasets into two categories according to the presence of myocardial motion. As a result, motion was found in 87 series (48.3%). If the myocardium was found by visual inspection to move between any two frames, this series was classified as "with motion." Only when the myocardium was still across all images, this series was classified as "no motion."

To quantify the performance of motion correction, two frames with good contrast between blood and myocardium were selected for every "with motion" series (87 series in total). For series where the myocardium was

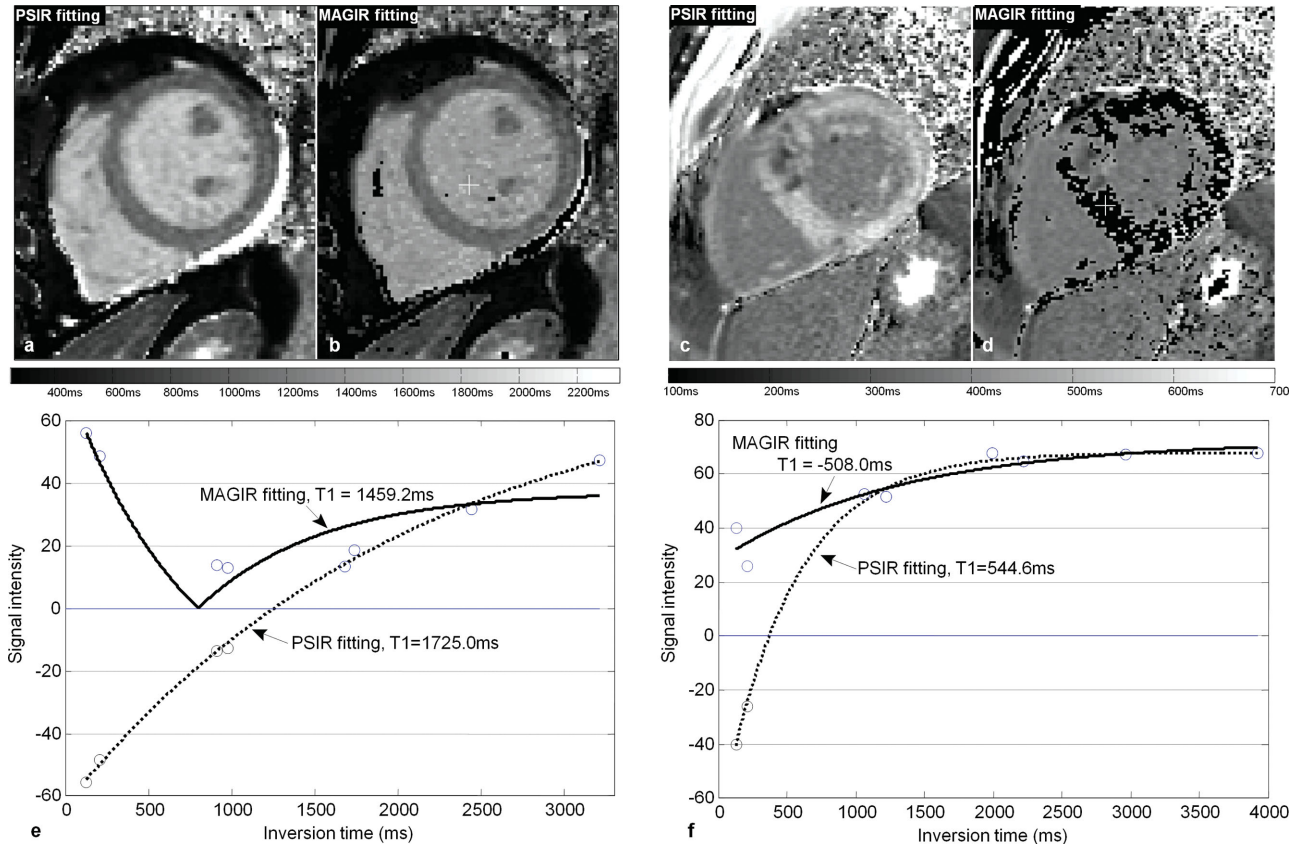

FIG. 6. MOLLI inversion recovery signal curves with MAGIR and PSIR fitting. Both strategies do not require the multiple trials to find the polarity for every data point. However, for postcontrast imaging with largely shortened T_1 values, there may not be sufficient number of data points sampled before the inversion, which frequently leads to the failure of MAGIR fitting. For the precontrast cases, this strategy often leads to inferior mapping quality. **a**: T_1 map of a precontrast MOLLI dataset using PSIR fitting. **b**: T_1 map estimated using the absolute magnitude fitting for the same dataset, showing underestimation of T_1s. **c**, **d**: T_1 map of a postcontrast MOLLI dataset using the PSIR and MAGIR fitting. The latter shows incorrect estimation of T_1. For the marked pixel, the estimated signal intensity curves are plotted with the sampled intensities for the precontrast (**e**) and postcontrast (**f**) cases. Especially in (f), the MAGIR fitting fails because only two data points are sampled before the nulling points, while the phase-sensitive fitting with the known signal polarity is much more robust against T_1 shortening.

stationary, 25 series were first randomly selected, and two frames were picked per stationary series.

For all selected frames, the myocardium was manually delineated by the reader, and the segmentation was propagated to the motion-corrected images using the deformation fields. Because the motion correction should improve the overlap of myocardium between those two selected frames, the Dice similarity coefficient (DSC) (17) was computed before and after motion correction. For two segmented regions A and B, the DSC is defined as:

$$\mathrm{DSC} = \frac{2 \times \mathrm{area}(A \cap B)}{\mathrm{area}(A) + \mathrm{area}(B)}$$

The maximal possible Dice coefficient is 1, indicating a perfect overlap. The false positive (FP) and false negative (FN) errors were also computed. FP is defined as the area ratio of region A that is not overlapped by region B (FP = area(A/B)/area(A)), and FN is defined as the area ratio of region B that is not overlapped by region A (FN = area(B/A)/area(B)).

To quantify the local nonrigid misalignment, a myocardium boundary error (MBE) was computed for all series. This measure is defined as the mean distance between endo- and epi-myocardial contours of two selected frames.

Previous studies (9) showed that for the anatomy with simple geometry such as myocardium, the inter-rater variability is not severe and reasonable inter-rater reproducibility can be achieved. The reported DSC for inter-rater variability test for myocardium segmentation is 0.853 ± 0.050 (computed on manual myocardial segmentation from two independent human raters), and the MBE is less than one pixel. Because a DSC measure above 0.7 indicates good agreement between two independent segmentations (18), in this study we did not further validate the inter-rater variability of myocardial segmentation.

Homogeneity of T_1 Estimation

With the hypothesis that PSIR fitting can lead to improved homogeneity of T_1 estimation, the homogeneity of T_1 maps was quantified by selecting a region of interest within the blood pool for all 180 series and computing the STD of T_1s. First, the blood has rather stable T_1 values. Second, with the injection of contrast, the T_1 of blood is uniformly shortened, which may not be true for other tissues. Third, compared to the myocardium, it is more robust to select a region of interest within the

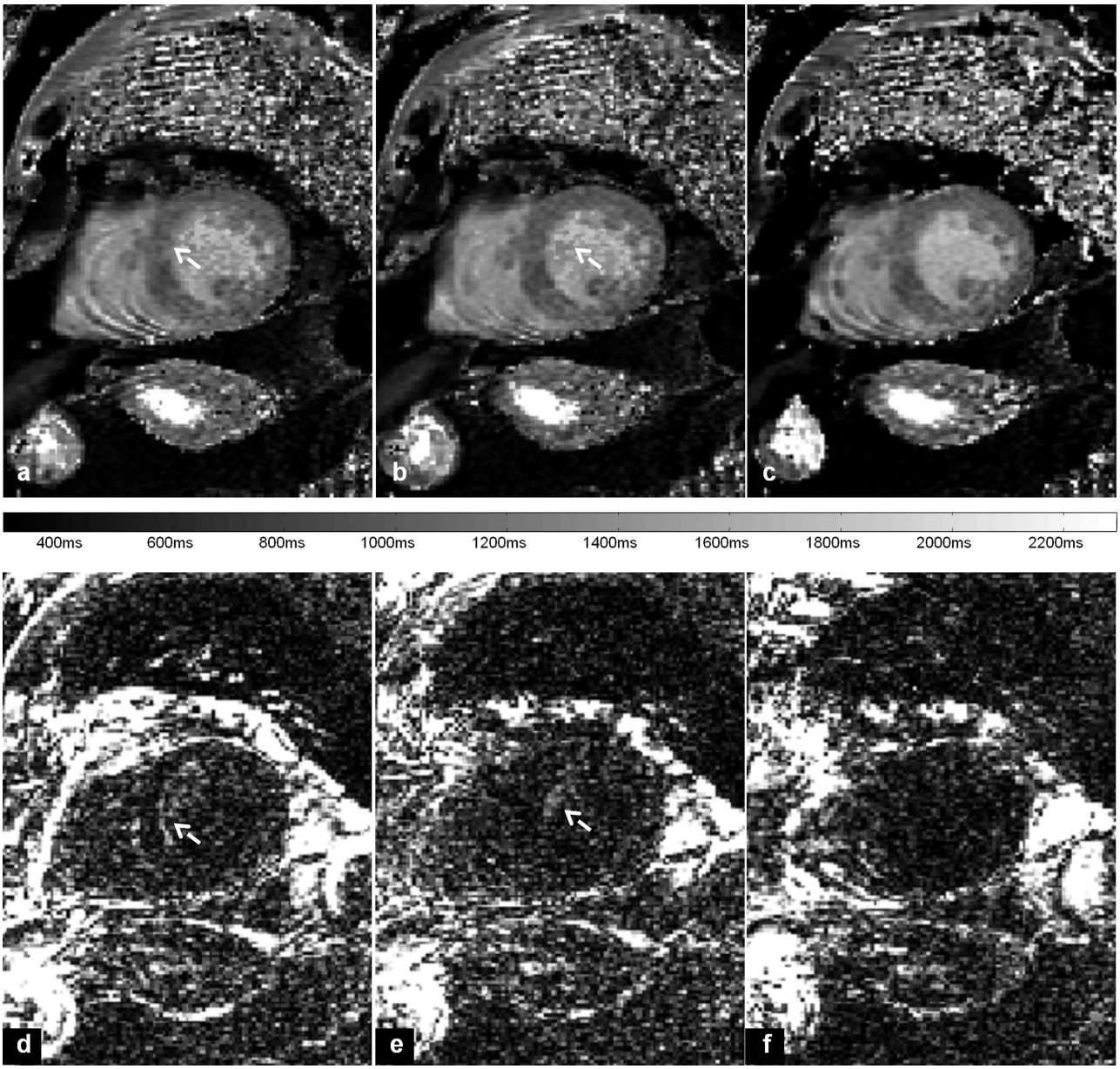

FIG. 7. T_1 maps and fitting residual errors of a precontrast dataset. **a**, **d**: T_1 map and fitting residuals without motion correction. **b**, **e**: T_1 map and residuals with SynMOCO and MF-MAGIR fitting. **c**, **f**: T_1 map and residuals with PSIR-MOCO and fitting. The residual plots are windowed at the identical level. Both SynMOCO and PSIR-MOCO have improved the boundary sharpness of T_1 map and reduced the residual along the septum wall. The PSIR fitting further reduce the residuals and leads to better T_1 homogeneity, compared to MF-MAGIR fitting.

blood pool to avoid the disturbance of motion. Finally, the T_1 homogeneity of the myocardium can be altered by potential pathologies, such as acute or chronic infarction or edema, while the blood T_1 is not. Thus, the fluctuation of T_1 estimation can be more precisely quantified within the blood pool. The homogeneity was measured for T_1 maps computed using PSIR fitting and MF-MAGIR fitting after the PSIR MOCO; thus, the influences of cardiac motion can be ignored and the effects of phase-sensitive fitting can be highlighted.

RESULTS

The necessity of motion correction for MOLLI T_1 mapping was confirmed by visual reading, as discernible motion was found in almost half of the entire data cohort. Examples of MOLLI motion correction are shown in Fig. 8, indicating the improved alignment of the myocardium.

Directly aligning MOLLI magnitude images without handling the largely varying image contrast can lead to frequent failures in image registration. To demonstrate this phenomenon, the middle frame of every series was picked as the reference to which all other frames were registered. Visual reading confirmed that unrealistic deformation or failed registration was found in 124 cases among the whole cohort (68.9%). This failure rate is too high to accept direct registration as a solution for MOLLI motion correction. A more robust motion correction is thus needed.

FIG. 8. Example of motion correction. **a–c**: A MOLLI series where myocardium shows noticeable motion. **d–f**: Results by directly applying the nonrigid registration shows the failure of registration. **g–i**: Results after SynMOCO. **j–l**: Results after PSIR-MOCO. Both SynMOCO and PSIR-MOCO are capable of correcting the heart motion. A total of three out of eight images are shown here.

For series with motion, the proposed method successfully corrects the myocardial movement (Fig. 8). The quantitative measures are reported in Table 1. The paired *t*-test was used to quantify the statistical significance. With the PSIR-MOCO, the DSC is increased significantly (0.870 ± 0.056, $P < 1\text{ e } -5$), compared to 0.812 ± 0.108 measured on the original MOLLI images. Consistently, both FP and FN are significantly decreased ($P < 1\text{ e } -5$ for both). The MBE is 1.476 ± 0.872 mm for original MOLLI and reduced to 0.981 ± 0.487 mm after PSIR motion correction.

For cases where the myocardium remains stationary, the PSIR-MOCO does not introduce unrealistic deformation and shows good robustness against the varying image contrast (Fig. 9). Table 2 summarizes the corresponding measures. The Dice coefficient which is originally 0.887 ± 0.026 remains stable after PSIR-MOCO (0.885 ± 0.027, $P = 0.408$). The FP and FN errors are almost unchanged. The original MBE is 0.935 ± 0.411 mm and after PSIR-MOCO, this measure is 0.920 ± 0.405mm ($P = 0.465$). These measures support the observation that unwanted deformation is not introduced by the PSIR-MOCO, indicating a reasonable degree of robustness.

The performance of PSIR-MOCO was compared to the SynMOCO. Both methods were reasonably robust against

Table 1
Quantitative Measures of Phase-Sensitive Motion Correction for MOLLI Series with Motion

	Dice			FP		
	ORI	PS	SYN	ORI	PS	SYN
Mean	0.812	0.870	0.864	0.197	0.143	0.149
STD	0.108	0.056	0.061	0.118	0.071	0.078
P value		ORI vs. PS: <1 e −5 ORI vs. SYN: <1 e −5 PS vs. SYN: 0.214			ORI vs. PS: <1 e −5 ORI vs. SYN: <1 e −5 PS vs. SYN: 0.247	
	FN			MBE (mm)		
	ORI	PS	SYN	ORI	PS	SYN
Mean	0.178	0.116	0.122	1.476	0.981	0.995
STD	0.110	0.061	0.065	0.872	0.487	0.446
P value		ORI vs. PS: <1 e −5 ORI vs. SYN: <1 e −5 PS vs. SYN: 0.235			ORI vs. PS: <1 e −5 ORI vs. SYN: <1 e −5 PS vs. SYN: 0.648	

ORI, original images; PS, phase-sensitive motion correction; SYN, synthetic image estimation-based motion correction.

rapid contrast changes and the overall performance was similar, as listed in Tables 1 and 2. The PSIR-MOCO is more efficient because synthetic images are not needed anymore. The SynMOCO utilizes the MF-MAGIR fitting for the estimation of synthetic images. Because a T_1 signal curve has to be estimated for each pixel in the synthetic image, the multiple fits required in the MF-MAGIR fitting actually consumed most computational time in the SynMOCO. On the contrary, the proposed scheme only needs one T_1 fitting after the motion correction. The PSIR-MOCO decouples the motion correction and parametric fitting because of its ability to recover the signal polarity. The computational time of PSIR T_1 fitting was found to be 4.4 ± 0.3 s per MOLLI series without the multithreading. For the MF-MAGIR fitting, the time cost was 13.6 ± 1.3 s per MOLLI series. With the use of multithreading (measurements were performed with 16 threads on eight cores with hyper-threading enabled), ~2× speedup was still achieved (0.93 ± 0.09 s per MOLLI series for PSIR fitting and 1.90 ± 0.19 s per MOLLI series for MF-MAGIR fitting). The entire processing of PSIR-MOCO and SynMOCO with multithreading took 6.43 ± 0.83 s and 11.8 ± 1.2 s per MOLLI series, including motion correction and T_1 fitting. The time cost for GRAPPA reconstruction was excluded because this step is required in both cases when parallel imaging is used. All MOLLI series includes eight inversion recovery images with the reconstructed image size 192 × 144.

To verify the performance on precontrast and postcontrast cases, quantitative measures were computed separately for precontrast and postcontrast series with motion. The DSC after PSIR-MOCO is 0.856 ± 0.072 for precontrast and 0.882 ± 0.035 for postcontrast ($P > 0.05$). The decreases of MBE errors after PSIR-MOCO were 0.648 ± 0.734 mm for precontrast and 0.375 ± 0.521 mm for postcontrast ($P > 0.05$). Significant deviation on motion correction performance was not found between precontrast or postcontrast imaging.

With effective motion correction, T_1 maps show reduced motion artifacts and improved boundary sharpness, as illustrated in Fig. 10. To demonstrate the insufficient robustness of MAGIR fitting (fitting using absolute magnitude signal), this strategy is applied to all images after the PSIR-MOCO, and T_1 maps are computed and reviewed visually. Clearly failed fitting within myocardium, similar to the one shown in Fig. 6d, were found in 81 series (45.0%), including 7 precontrast and 74 postcontrast series. This high rate of failure indicates the insufficient performance of MAGIR fitting strategy, especially for postcontrast scenario. For the precontrast cases, the map quality is often degraded due to local minima, which trap the nonlinear optimization (e.g., Fig. 6b). Better approaches to achieve stable T_1 estimation such as MF-MAGIR or PSIR fitting are necessary.

Compared to the MF-MAGIR, the PSIR fitting is not only considerable faster but also leads to less fluctuation of T_1 estimates. The MF-MAGIR fitting leads to a STD of 60.594 ± 23.784 ms for precontrast and 17.876 ± 7.371 ms for postcontrast series. With the PSIR fitting, statistically significant changes were found for both precontarst and postcontrast T_1s (precontrast, 57.804 ± 21.872 ms, paired *t*-test, $P < 1$ e −4; postcontrast, 15.519 ± 6.224 ms, $P < 1$ e −5). The measured STDs were shown in Fig. 11. The mean T_1 values estimated with both fitting approaches remain statistically unchanged (precontrast: 1520.175 ± 152.642 ms for MF-MAGIR and 1517.459 ± 150.903 ms for PSIR; postcontrast: 319.007 ± 70.061 for MF-MAGIR and 318.272 ± 69.835ms for PSIR, $P > 0.1$ for all cases). Additionally, a human rater reviewed the T_1 maps generated with both methods for all 180 series. Compared to the MF-MAGIR fitting, the PSIR fitting leads to visible improvements in 83 series (46.1%), including 34 precontrast and 49 postcontrast series. This observation is consistent with the quantitative results that favor the improved fitting with PSIR.

DISCUSSION

While the feasibility of myocardial T_1 mapping using MOLLI imaging sequences and related variations has

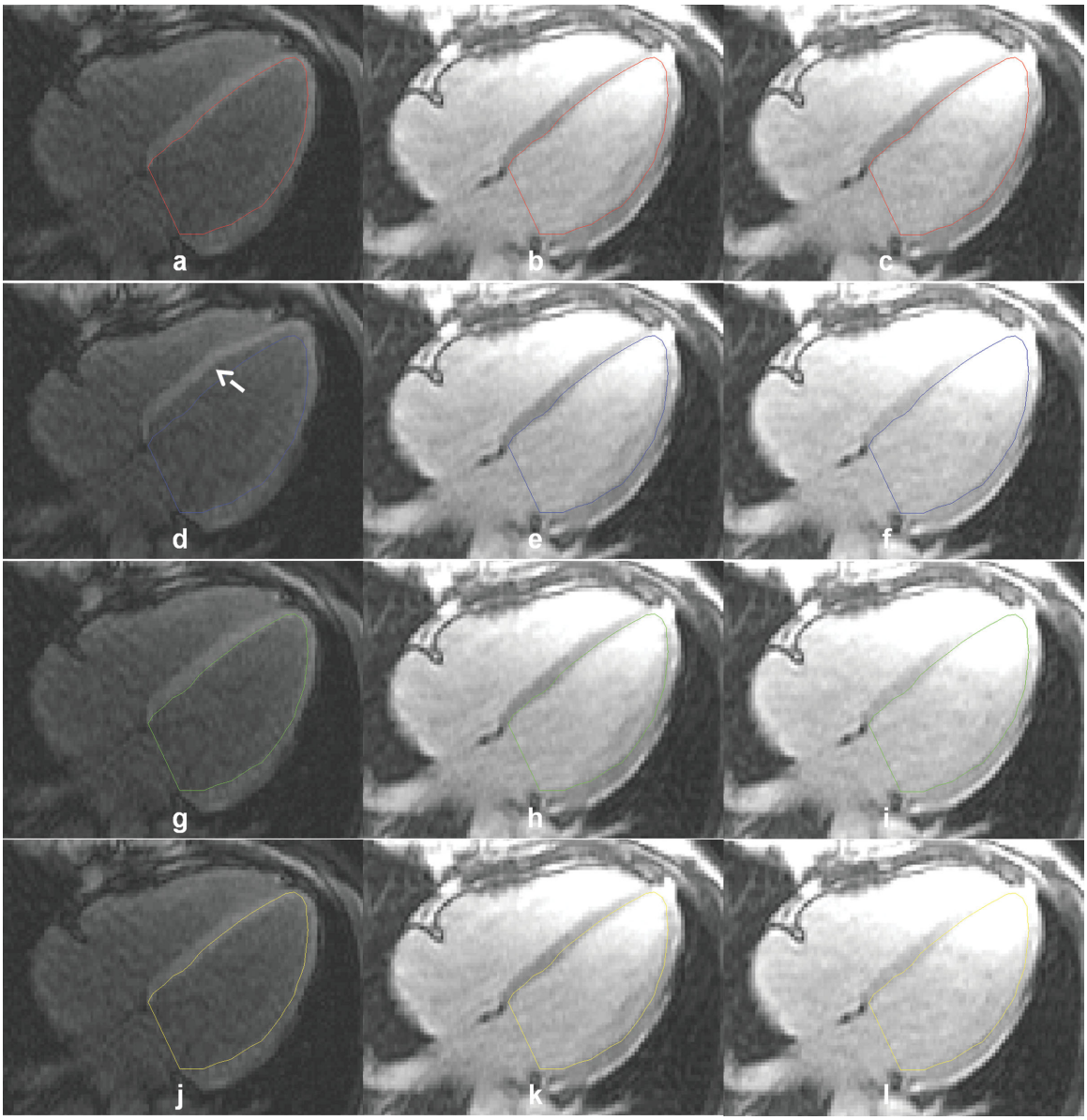

FIG. 9. Example of MOLLI motion correction. **a–c**: Original MOLLI images in studies for which the myocardium is "stationary." **d–f**: Results by directly applying the nonrigid registration. The unrealistic deformations caused by failed registration can be observed around the septum (arrow) in (d). **g–i**: Results after SynMOCO. **j–l**: Results after PSIR-MOCO.

been proven by previous studies, the undesired patient movement or imperfect breath-holding often impair the mapping quality. Severe heart motion can lead to significant bias in the estimated T_1s. To correct the myocardium motion and improve the quality of T_1 mapping, a novel motion correction and T_1 estimation scheme is proposed. The specialty of this method lies on utilizing the phase-sensitive reconstruction. In this way, the polarity of inversion recovery magnetization is restored and the contrast inversion among MOLLI images is avoided. Robust motion correction can thus be achieved. Moreover, the known signal polarity eliminates the need for time-consuming multitrial fitting. The performance of proposed technique was evaluated in vivo on a cohort of 45 patients. We have shown that this scheme leads to very robust motion correction and does not introduce unrealistic deformation.

To efficiently utilize the phase-sensitive reconstruction, we make the assumption that the background phase can be readily estimated from the MOLLI images with the longest TI even at the high heart rates with the longest T_1s (i.e., precontrast administration). Given the current imaging protocol, the magnetization will be well recovered after five heartbeats for the postcontrast scenario. For the precontrast imaging cases, if the heart rate is within the common range (e.g., $<$100) which holds true for most subjects, our experiments show that the background phase can be well estimated. If the heart rate is further increased, it will quickly become impractical to perform MOLLI imaging since the single shot images do not have sufficient imaging window, and image quality will be degraded by motion blurring. To conduct MOLLI imaging for very high heart rate, the imaging matrix size has to be reduced, and more heart

Table 2
Quantitative Measures of Phase-Sensitive Motion Correction for MOLLI Series Without Motion

	Dice			FP		
	ORI	PS	SYN	ORI	PS	SYN
Mean	0.887	0.885	0.882	0.103	0.108	0.109
STD	0.026	0.027	0.029	0.045	0.049	0.049
P value		ORI vs. PS: 0.408 ORI vs. SYN: 0.116 PS vs. SYN: 0.248			ORI vs. PS: 0.118 ORI vs. SYN: 0.050 PS vs. SYN: 0.700	
	FN			MBE (mm)		
	ORI	PS	SYN	ORI	PS	SYN
Mean	0.123	0.123	0.127	0.935	0.920	0.948
STD	0.047	0.045	0.050	0.411	0.405	0.525
P value		ORI vs. PS: 0.962 ORI vs. SYN: 0.340 PS vs. SYN: 0.218			ORI vs. PS: 0.465 ORI vs. SYN: 0.677 PS vs. SYN: 0.357	

ORI, original images; PS, phase-sensitive motion correction; SYN, synthetic image estimation-based motion correction.

rates beats shall be allowed for good recovery of magnetization.

The imaging protocols used in this study requires one breath-hold lasting 11 heartbeats. While this is achievable in clinical setting, our experiments show that more than 60% of the acquired series present discernible motion. This observation highlights the necessity for either shortening the imaging protocol or even conducting free-breathing acquisition. The recently published shortened-MOLLI protocol (shortened-MOLLI; Ref. 4) proposes to acquire a shorter MOLLI series for T_1 mapping (nine heartbeats). This strategy can slightly reduce the sensitivity to breathing motion at the cost of decreased signal-to-noise ratio because less data points are used for curve fitting. More evaluation is needed to further optimize the MOLLI imaging protocol and pursue better tradeoff between total acquisition time, signal-to-noise ratio of T_1 map and sensitivity to patient motion.

The proposed method has some potential to correct in-plane motion of myocardium in a free-breathing acquisition; but it may not be capable of correcting large through-plane motion as current image registration is performed on 2D frames. Its applicability on datasets with large *R–R* interval variations, such as arrhythmias, may be limited. One possible extension to make the proposed method handle free-breathing MOLLI could be detecting and excluding frames with strong through-plane motion from fitting and registration. The cost here may include an increased number of acquired heartbeats and IR images.

Compared to MAGIR fitting, the PSIR fitting is similarly efficient but much more robust against the data sampling pattern along the IR curve because the signal polarity can be determined before the nonlinear optimization. As illustrated in Fig. 6, the fitting on absolute magnitude signals leads to error-prone estimation of T_1 values. The accuracy of MAGIR fitting might be improved with better initialization; however, the T_1s within the field of view experience significant variations for different tissue types and contrast concentration. The TIs of MOLLI acquisition depend on the heart rate as well. As a result, there is no clear solution to constraint the data sampling along the inversion recovery curve to favor the magnitude fitting. One possible way might be to apply a brute-force search among possible combinations of A, B, and T_1^* to find a better starting point, but it will prolong the parametric estimation.

The proposed PSIR fitting is much faster than the MF-MAGIR fitting. Depending on the T_1 of a pixel and the TIs, the PSIR fitting can reduce ambiguity for whether to invert signal points near the zero-crossing of magnetization. The multiple trial strategy may not always assign the correct polarity for these points, while the phase-sensitive reconstruction readily provides this information. Furthermore, the influences of MOLLI signal points on the final T_1 estimate depend on the derivative magnitude of the inversion recovery curve at the corresponding TIs. For example, the magnitude of IR recovery derivative is larger for shorter TI and quickly decreases for longer TI (the derivative of IR recovery is $2e^{(-\mathrm{TI}/T_1)}/T_1$). Thus, the signal points sampled at the beginning period of IR recovery can have more influences on the final T_1 estimate. This may indicate that the improvement of PSIR fitting on the T_1 mapping is more prominent for postcontrast cases than for precontrast, as the former has significantly shortened T_1 values.

For the experiments conducted in this article, the T_1 value is computed as $T_1^*(x,y) \times (B(x,y)/A(x,y) - 1)$, following the suggestion of the original MOLLI sequence paper (1). Given the balanced SSFP readout in current MOLLI experiments, this formula can lead to underestimation of real T_1s, as reported in Ref. 1. More precise formula specifically considering SSFP readout scheme could further improve the T_1 estimate. On the other hand, the potential benefits of PSIR T_1 mapping, including more accurate signal polarity determination and robust motion correction, are independent of the correction of apparent T_1^*. With the known signal polarity, the ambiguity of whether to invert signal points around magnetization nulling is removed.

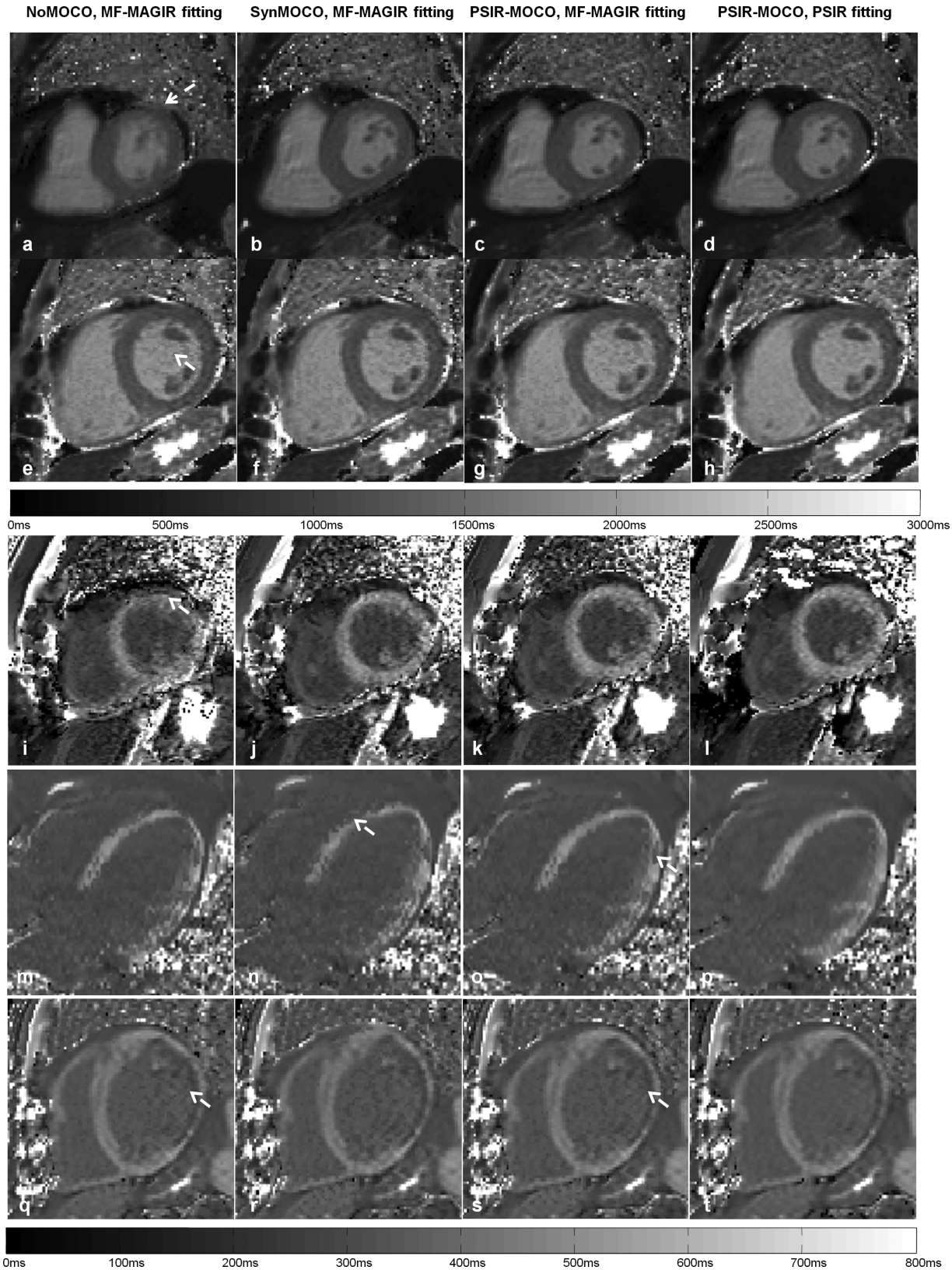

FIG. 10. T_1 maps of precontrast (**a**–**h**) and postcontrast (**i**–**t**) MOLLI series. The first column (a, e, i, m, q) shows the T_1 maps without motion correction. The second column (b, f, j, n, r) is with SynMOCO. The third (c, g, k, o, s) and fourth columns (d, h, l, p, t) are generated after PSIR-MOCO. The first, second, and third columns are produced with MF-MAGIR fitting, and the last column is with PSIR fitting. With motion correction (more prominent for the first and third rows), the motion blurring is reduced, and myocardial boundary sharpness is improved. For cases where there is very little cardiac motion, e.g., the second and fifth rows, the motion correction does not introduce unwanted deformation or lead to degraded mapping quality. Comparing the fitting method (columns 3 and 4) for a given motion correction scheme (PSIR-MOCO), the PSIR T_1 fitting (the last column) improves the T_1 estimation (e.g., the second, fourth, and fifth rows) as compared to the MF-MAGIR fitting (the third column).

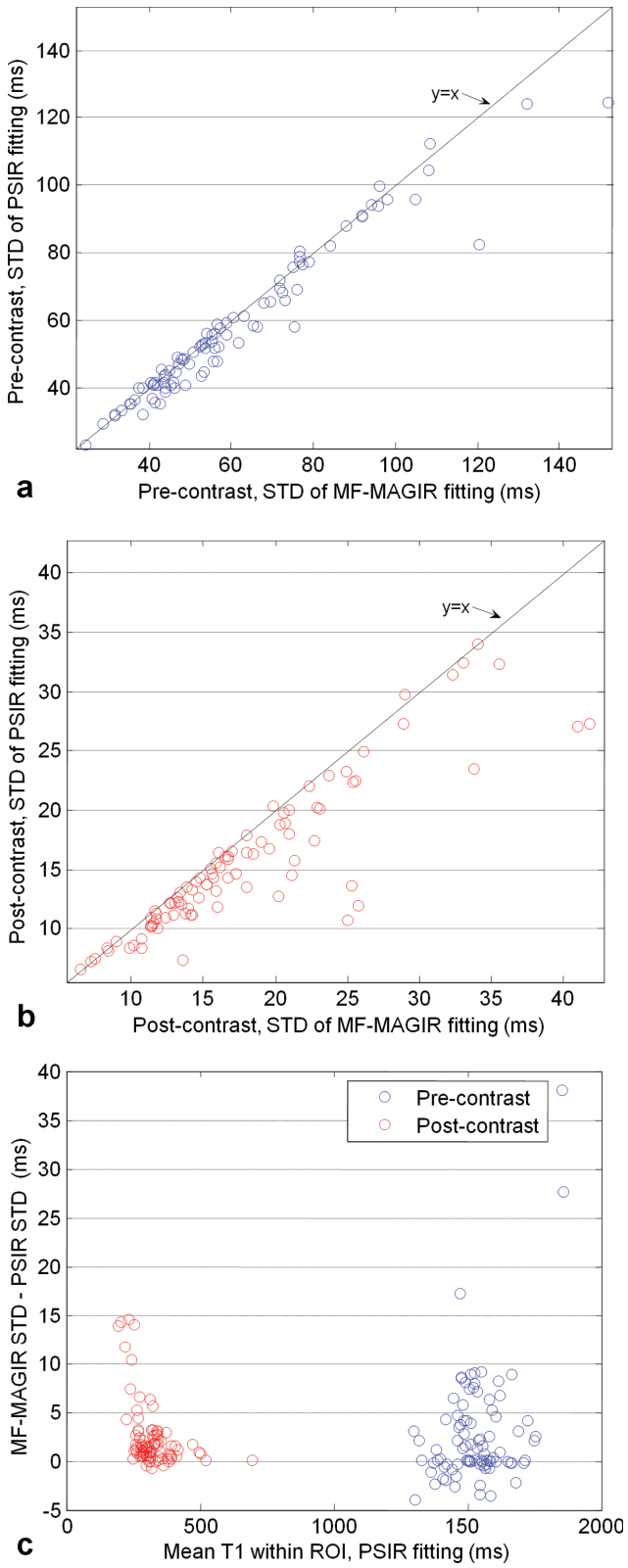

FIG. 11. Measured STD of T_1 values (ms) for a region in the blood pool comparing MF-MAGIR and PSIR fitting for (**a**) precontrast and (**b**) postcontrast MOLLI series. The phase-sensitive fitting leads to more uniform T_1 estimation in the blood pool region of interest. **c**: The plot of the difference between STD of T_1 obtained with MF-MAGIR minus the STD for PSIR fitting shows that the MF-MAGIR tends to have greater variation for both precontrast and postcontrast cases.

CONCLUSIONS

We have presented a novel scheme to perform the motion correction and parametric fitting for myocardial T_1 mapping. The key idea is to restore the signal polarity of inversion recovery magnetization using phase-sensitive reconstruction. This method is fully automated and does not require any preprocessing. The in vivo validation on a data cohort of 45 patients illustrates the robustness of the proposed method. The PSIR fitting with the restored signal polarity can further improve the mapping process with decreased computational cost and improved T_1 estimation.

REFERENCES

1. Messroghli DR, Radjenovic A, Kozerke S, Higgins DM, Sivananthan MU, Ridgway JP. Modified Look-Locker inversion recovery (MOLLI) for high-resolution T1 mapping of the heart. Magn Reson Med 2004;52:141–146.
2. Messroghli DR, Plein S, Higgins DM, Walters K, Jones TR, Ridgway JP, Sivananthan MU. Human myocardium: single-breath-hold MR T1 mapping with high spatial resolution—reproducibility study. Radiology 2006;238:1004–1012.
3. Ferreira V, Piechnik S, Dall'Armellina E, Karamitsos T, Francis J, Friedrich M, Robson M, Neubauer S. Quantification of acute myocardial injury by ShMOLLI T1-Mapping, T2-weighted and late gadolinium imaging in patients presenting with chest pain, positive troponins and non-obstructive coronary arteries. J Cardiovasc Magn Reson 2011;13(suppl 1):P16.
4. Piechnik S, Ferreira V, Dall'Armellina E, Cochlin L, Greiser A, Neubauer S, Robson M. Shortened modified Look-Locker inversion recovery (ShMOLLI) for clinical myocardial T1-mapping at 1.5 and 3T within a 9 heartbeat breathhold. J Cardiovasc Magn Reson 2010;12:69.
5. Deichmann R. Fast high-resolution T1 mapping of the human brain. Magn Reson Med 2005;54:20–27.
6. Gold GE, Han E, Stainsby J, Wright G, Brittain J, Beaulieu C. Musculoskeletal MRI at 3.0 T: relaxation times and image contrast. Am J Roentgenol 2004;183:343–351.
7. Flacke SJ, Fischer SE, Lorenz CH. Measurement of the gadopentetate dimeglumine partition coefficient in human myocardium in vivo: normal distribution and elevation in acute and chronic infarction. Radiology 2001;218:703–710.
8. Ugander M, Bagi P, Oki A, Chen B, Hsu L-Y, Aletras A, Shah S, Greiser A, Kellman P, Arai A. Quantitative T1-maps delineate myocardium at risk as accurately as T2-maps—experimental validation with microspheres. J Cardiovasc Magn Reson 2011;13(suppl 1):O62.
9. Xue H, Shah S, Greiser A, Guetter C, Littmann A, Jolly M-P, Arai AE, Zuehlsdorff S, Guehring J, Kellman P. Motion correction for myocardial T1 mapping using image registration with synthetic image estimation. Magn Reson Med 2012;67:1644–1655.
10. Sass M, Ziessow D. Error analysis for optimized inversion recovery spin-lattice relaxation measurements. J Magn Reson 1977;25:263–276.
11. Nekolla S, Gneiting T, Syha J, Deichmann R, Haase A. T1 maps by K-space reduced snapshot-FLASH MRI. J Comput Assist Tomography 1992;16:327–332.
12. Kellman P, Arai AE, McVeigh ER, Aletras AH. Phase-sensitive inversion recovery for detecting myocardial infarction using gadolinium-delayed hyperenhancement. Magn Reson Med 2002;47:372–383.
13. Chefd'hotel C, Hermosillo G, Faugeras O. Flows of diffeomorphisms for multimodal image registration. In Proceedings of IEEE International Symposium on Biomedical Imaging, Washington, DC, USA, 2002. p. 753–756.
14. Guetter C, Hui X, Chefd'hotel C, Guehring J. Efficient symmetric and inverse-consistent deformable registration through interleaved optimization. In Proceedings of IEEE International Symposium on Biomedical Imaging, Chicago, IL, USA, 2011. p. 590–593.
15. Nelder JA, Mead R. A simplex method for function minimization. Comput J 1965;7:308–313.
16. Marquardt DW. An algorithm for least-squares estimation of nonlinear parameters. J Soc Ind Appl Math 1963;11:431–441.
17. Dice LR. Measures of the amount of ecologic association between species. Ecology 1945;26:297–302.
18. Zijdenbos AP, Dawant BM, Margolin RA, Palmer AC. Morphometric analysis of white matter lesions in MR images: method and validation. IEEE Trans Med Imaging 1994;13:716–724.